Theor. Comput. Fluid Dyn.
https://doi.org/10.1007/s00162-023-00659-w


ORIGINAL ARTICLE

**Xianzhang Xu · Antonios Gementzopoulos · Girguis Sedky · Anya R. Jones · Francis D. Lagor**

# Design of optimal wing maneuvers in a transverse gust encounter through iterated simulation or experiment

Received: 15 February 2023 / Accepted: 2 June 2023


**Abstract** Wing–gust encounters cause harmful lift transients that can be mitigated through maneuvering of the wing. This paper presents a method to generate an open-loop (i.e., prescribed) maneuver that optimally regulates the lift on the wing during a transverse gust encounter. Obtaining an optimal maneuver is important for laboratory experiments on the physics of wing–gust interactions and may be useful for the future design of feedback controllers. Prior work of the authors has shown that an Iterative Maneuver Optimization (IMO) framework can generate an optimal maneuver by using a surrogate model to propose a control signal that is then tested in experiment or high-fidelity simulation. The input to the surrogate model is updated to account for differences between the test data and the expected output. The optimal maneuver is obtained through iteration of this process. This paper simplifies the IMO method by replacing the surrogate model with the classical lift model of Theodorsen, removing the process of optimization over the surrogate model, and removing the requirement to know the time-averaged profile of the gust. The proposed method, referred to as Simplified IMO (SIMO), only requires input and output data collected from simulations or experiments that interact with the gust. Numerical simulations using a Leading Edge Suction Parameter modulated Discrete Vortex Model are presented to generate the input and output data of the wing–gust encounters for this paper. Experiments in a towing tank also validated the SIMO method. The results show an optimal pitch maneuver and an optimal plunge maneuver that can each regulate lift during a transverse gust encounter.

**Keywords** Gust mitigation · Wing maneuvers · Discrete vortex model · Optimal control

## 1 Introduction

Gust encounters can de-stabilize the flight of small, unmanned aerial vehicles and lead to significant damage [1,2]. Consequently, wing motions and wing–gust encounters have been studied with great interest at low Reynolds numbers (e.g., see [3–5]). Existing atmospheric flight controllers perform model-based control in unsteady flow environments by treating the gust as a disturbance input that can be rejected through linear robust-control techniques [6–8]. However, these vehicles often encounter transverse gusts that can produce large disturbances and induce shedding of coherent flow structures that greatly influence the aerodynamic forces

Communicated by Ashok Gopalarathnam.

X. Xu · F. D. Lagor (✉)
Department of Mechanical and Aerospace Engineering, University at Buffalo, The State University of New York, Buffalo, NY 14260, USA

F. D. Lagor
E-mail: flagor@buffalo.edu

A. Gementzopoulos · G. Sedky · A. R. Jones
Department of Aerospace Engineering, University of Maryland, College Park, MD 20742, USA

Published online: 15 June 2023

[9,10]. Hence, more recent studies have investigated the structure of the flow field during transverse wing–gust encounters at low Reynolds numbers in both high-fidelity numerical simulations [11,12] and experiments [13]. Findings indicate that large-amplitude transverse gusts can cause massive flow separation, resulting in deviation of the lift force from its steady value prior to the encounter. Often, a large lift overshoot occurs early in the encounter, and a lift deficit can occur while exiting the gust. Many attempts to mitigate the effects of the gust have focused on maneuvering the wing [14–16]. Maneuvering the wing can influence the circulatory, non-circulatory, and added-mass contributions to the lift force by altering the wing's orientation and rates of change during the encounter [4]. Sedky [17], and Andreu-Angulo and Babinsky [14] have shown that pitch maneuvers can regulate lift near either zero or nonzero values.

Minimizing absolute deviations of the lift from a reference value is a regulation problem in the study of control. There are many modern control techniques to address regulation problems for linear and nonlinear systems. However, many of these tools are model-based and would require modeling and identification (i.e., quantifying parameters) of the wing–gust system prior to use. Poor modeling or system identification can lead to poor performance of the controller, and even instability of the closed-loop system. Proportional-Integral-Derivative (PID) controllers can often work for control problems in which the system model is uncertain or unknown. However, to obtain performance guarantees for a PID controller requires a system model for closed-loop analysis.

In wing–gust encounters, the fluid system has unsteady, nonlinear, and multi-scale dynamics, which makes capturing all relevant physical effects difficult. Recent works in gust-encounter research have sought low-order models for the wing–gust interaction for the purposes of interpreting experimental data through the lens of the model [4], designing feedback controllers [15], and designing prescribed maneuvers [14,16]. Early potential-flow models of wing–gust encounters developed by Wagner, Theodorsen, Küssner, and von Kármán [18–21] have been examined for applicability to large-amplitude gusts. Andreu-Angulo and Babinsky [14], as well as Sedky et al. [22], combined different classic aerodynamic theories to model the effects of gust and wing kinematics. They used their model to design a maneuver that maintains a specified effective angle of attack during the encounter. These models provide some useful, predictive capability, despite assumptions of low-frequency motion and attached flow.

To include external vorticity in a potential-flow model, Corkery et al. [23] modeled the shear layers of a transverse gust using discretized vortex sheets to study the forces on the wing. Since shed vorticity, such as the Leading Edge Vortex (LEV), can greatly impact the lift force [24,25], some studies simulate wing–gust encounters using a Discrete Vortex Model (DVM) in which vortices freely advect within a potential flow model. Andreu-Angulo and Babinsky [26] used a DVM to design a prescribed maneuver by pitching the wing to zero out the lift calculated within the model at each time step. Sedky et al. [27] used a DVM to assess the performance of a proportional feedback controller that was tuned using Theodorsen's unsteady aerodynamic model. In prior work [16], the authors designed an optimal pitching maneuver for a nonlinear, modified Goman–Khrabrov (mGK) model [28] of a gust encounter using an optimal-control framework based on a gradient-descent approach. These works demonstrate lift regulation with appropriate wing maneuvers; however, lift forces still experience deviations from the desired reference value when the profile is applied in experiment or high-fidelity simulation. These deviations are attributable to unmodeled effects, because the prescribed profile or feedback controller is subject to the limitations of the model used in its construction.

To study mechanisms of force mitigation through wing maneuvering, it is desirable to use a motion profile that is truly optimal, or at least as nearly optimal as possible. An optimal maneuver may provide valuable insight into wing–gust interaction that may inform future design of feedback controllers. Hence, the goal of this paper is to create a reliable method for off-line calculation of open-loop optimal maneuvers that can be utilized in experimental and computational research. In addition, we seek to reduce dependence on the model used during maneuver construction. One way to accomplish this goal is by incorporating experimental or high-fidelity simulation data from the system under study during maneuver construction. Several previous works [29–31] have used experimental data to generate optimal maneuvers in fluid-dynamic studies. Milano and Gharib [29] utilized a genetic algorithm to develop a pitch maneuver experimentally, with the goal of enhancing the average lift force generated. They established a correlation between maximizing the wing's force and maximizing the Leading Edge Vortex's (LEV) circulation strength. Similar experimental measurements were conducted by Peng and Milano [30] to identify key parameters affecting the optimal lift trajectory. Quinn et al. [31] maximized the propulsive efficiency of a heaving and pitching flexible panel using a gradient-based optimization. Using iterative experiments, Quinn et al. demonstrated how to optimize an aerodynamic force objective and study the physical mechanisms involved in force production. This type of optimization has not yet been applied to gust encounters.

Data-driven methods, such as Proper Orthogonal Decomposition (POD) [32] and Dynamic Mode Decomposition (DMD) [33], have become important tools for the analysis and reduced-order modeling of fluid systems [34]. These algorithms can provide an accurate, linear representation of the system. Extensions of the DMD algorithm have also addressed nonlinearities [35] and can include control inputs [36]. Unfortunately, identified linear control models are only valid at (or very close to) the prescribed inputs used in model construction. Changes in actuation require changes in the system model, which makes use of these approaches in optimal-control calculations difficult. Deem et al. [37] used an adaptive Linear-Quadratic Regulator (LQR) controller with the online DMD algorithm that updates the system model as new data arrives. Deem et al. [37] note that the control input is not optimal due to nonlinearity and time-varying features of the fluid system. Addressing the time-varying nature of a fluid system in construction of an optimal control signal may be possible if the flow is highly repeatable in experiment or simulation.

Rather than online construction of an optimal control, repeated experiments or simulations can provide data for offline refinement of the control. Some data-driven control methods tune the control signal in an iterative manner, such as Iterative Feedback Tuning (IFT) [38] and Iterative Learning Control (ILC) [39]. These methods use the error between the output signal and a desired output signal to update the control design or a reference signal for the controller in the next iteration. An iteration in either of these methods consists of applying the updated controller or control signal in experiment or high-fidelity simulation. IFT uses the output error information to adjust controller gains, while ILC uses the output error to adjust a reference input signal. In the authors' prior work [40], a method similar to ILC, called Iterative Maneuver Optimization (IMO), is applied to generate optimal maneuvers of a wing in a gust encounter through iterated experiments. The fundamental principle behind IMO is the same as ILC. However, the methods differ, because ILC typically applies to linear systems and uses a learning filter for the signal update, while IMO performs control signal updates by solving an optimal control calculation using a surrogate model.

The IMO method uses an optimal control calculation on an mGK model and several iterations through experiment or higher-fidelity simulation to generate an optimal maneuver for the true wing–gust system. In [40], the authors show that the mGK model produces an undesirable delay in the lift response during a gust encounter. However, the IMO method is able to overcome this deficiency to produce an optimal maneuver in simulation and a highly optimized maneuver in experiment. Although the IMO method is very useful, it has several limitations. In particular, the IMO method requires prior knowledge of the gust profile to derive the optimal control input using the mGK model. The mGK model also contains empirical terms that must be fit using initial experiments. Lastly, the optimal control procedure is slow and complex. The main objective of this paper is to simplify the IMO method.

This paper creates an iterative procedure that the authors refer to as Simplified IMO (SIMO). SIMO uses the classic unsteady lift model of Theodorsen [18] to predict the lift from the wing's maneuvers. Theodorsen's lift model includes pitching and plunging effects, as well as a term that accounts for wake vorticity. Brunton et al. [41] previously designed a controller by taking the Laplace transformation of Theodorsen's function to obtain transfer functions from the maneuver inputs to lift. Sedky et al. [27] considered the transverse gust as an output disturbance and designed an output-feedback controller based on robustness arguments and the sensitivity transfer function. This approach successfully removes the requirement for prior knowledge of the gust profile, but it still requires an anticipated reduced-frequency range for the gust disturbance. In this paper, the SIMO method utilizes Theodorsen's lift model to replace the mGK surrogate model in IMO and designs output-feedback controllers for Theodorsen's pitch and plunge models to track a reference lift signal. The optimal maneuvers that regulate the lift of the wing during the transverse gust encounter are generated through an iterative approach and do not require any prior knowledge of the gust. Pitch acceleration and plunge acceleration inputs are studied individually using a DVM simulation with leading edge shedding modulated by the Leading Edge Suction Parameter (LESP) as the test system. This form of DVM is referred to in this paper as an LDVM.

The contributions of this paper are: (1) a method to construct an optimal lift-regulating maneuver in a transverse gust encounter based on Theodorsen's unsteady lift model and iterated experimentation, (2) determination of an optimal lift-regulating maneuver using a plunge input in numerical simulation with an LDVM simulation, and (3) experimental validation via force measurements of the proposed method for pitch and plunge inputs individually. These contributions are important because the simplified method for maneuver optimization greatly reduces the experimentation effort required by removing the need to initially characterize the wing and the gust (i.e., to empirically determine coefficients and the time-averaged gust profile). Additionally, examination of a plunge input expands on the previous work of the authors that only examined a pitching input in the IMO process.

This paper is organized as follows: Sect. 2 reviews the LDVM modeling technique for simulation of wing–gust encounters. Section 3 reviews the IMO method for determining an optimal maneuver for force regulation. Section 4 presents the framework of the Simplified IMO method and its application to design pitch or plunge maneuvers for lift regulation. Section 5 presents simulation results and discusses the relative merits and disadvantages of the SIMO method. Section 6 shows the experiment results of pitch and plunge maneuvers. Section 7 concludes the paper and discusses future work.

## 2 Discrete vortex model of wing–gust encounters

Discrete Vortex Models (DVMs) have been extensively used in modeling unsteady aerodynamic phenomena, such as formation and shedding of the Leading Edge Vortex (LEV) [25,42,43]. DVM methods are able to produce flow fields that closely agree with Computational Fluid Dynamics (CFD) simulations and experiments for fluid problems, such as LEV formation, dynamic stall, and high angle-of-attack motion [25,42–44]. Recent research [27,45] has employed DVM methods to model fluid dynamic problems with external flow disturbances. For example, SureshBabu et al. [45] investigated a maneuvering airfoil encountering a flow disturbance generated by an upstream cylinder through numerical simulation with a DVM model. DVM methods have also been utilized to model wing–gust encounters. As discussed by [27], a gust can be modeled using a prescribed velocity field that does not deform according to the wing's motion, or can be modeled using free vortices initially aligned in the shape of the gust that subsequently deform with the wing's motion. For the gust studied in [27], only minor differences in the lift prediction were noticed between these two approaches, but the prescribed velocity field approach provided significant computational savings.

A DVM is selected to model the gust encounter, because it is able to represent shedding of vorticity in response to a prescribed velocity field of the gust. The non-dimensional LESP quantity introduced by Ramesh et al. [25] serves as the criterion of leading-edge shedding. When the LESP value exceeds the critical value, LESPc, which is determined empirically from experimental or CFD data, the airfoil sheds vortices from the leading edge. The trailing edge of the airfoil continuously sheds vortices. This method was built on the time-stepping approach introduced by Katz and Plotkin [24]. At each time step, the DVM determines the distribution of vorticity at a discrete set of points along the chord of the airfoil in order to enforce no flow across the chord line. The DVM also sheds new vortices into the flow with strengths that are calculated to satisfy the Kelvin condition, which ensures that there is no net change in circulation in the airfoil and external flow field [25,45]. In this paper, the LDVM method is taken as the numerical simulation tool, and the gust effects are considered as an external flow disturbance incorporated in the downwash. The DVM sheds vorticity at the trailing edge at each time step, and it sheds vorticity at the leading edge if the LESP value is above the critical value LESPc. The detailed derivation of the LDVM method is omitted but is available in [25,46,47]. Similar to [48], the LESP expression used in this paper contains the effects of wing motion, since the LDVM method is slightly modified from [25]. Details of the LDVM simulation are shown in [47], where the Fourier coefficient $A_0$ is calculated using the downwash from an effective angle of attack expression in [49] that includes the motion kinematics and external flow effects (i.e., gusts).

Hemati et al. [50] previously noted that DVM models tend to over-predict the lift force. Dividing the normal force and the suction force by the dynamic pressure $\rho c U^2/2$ leads to the $2\pi$ lift-coefficient slope from classical thin-airfoil theory. In [40], the authors replaced the $2\pi$ coefficient with the empirical coefficient obtained from the steady-lift curve measured in experiments. The same modification is made in this paper to provide realistic lift values. Note that this modification only scales the output of the DVM simulation, which is a placeholder for experimental evaluation, and it does not alter the SIMO method. In particular, the SIMO method does not require empirical values.

The LDVM simulation of a wing's shed vorticity with a prescribed velocity profile of a transverse gust is presented in Fig. 1. The gust profile is based on time-averaged measurements of an experimental gust setup in a water towing tank at the University of Maryland, according to data from [40]. The lift coefficient $C_L$ is defined as the lift force divided by the dynamic pressure $\rho c U^2/2$, and the convective time is defined as $t^* = Ut/c$. A gray line in Fig. 1 provides the gust profile, which has a trapezoidal shape and an approximate gust ratio of $\mathrm{GR} = V_{\max}/U = 0.7$. The gust profile shown as a gray line represents the gust velocity seen by the leading edge. Note that the wing is still influenced by the gust after the leading edge exits the gust profile, since a portion of the wing is still within the gust. Within the LDVM simulation, the gust profile influences the downwash calculation, which in turn, influences vortex shedding and the forces on the wing. The gust profile is assumed to be unaffected by the wing, since Sedky et al. [27] have shown that simulated gust deformation does

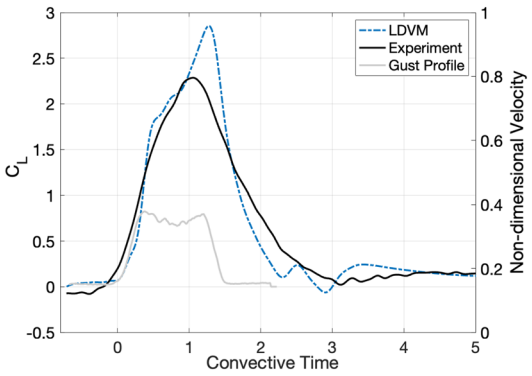


**Fig. 1** Lift coefficient of a non-maneuvering wing during an encounter with a trapezoidal, transverse gust (experimental data taken from [40])

not significantly alter the forces when compared to an encounter with a non-deforming gust profile at a similar Reynolds number and gust ratio. Figure 1 also shows the lift coefficient during an LDVM simulation of a gust encounter for a non-maneuvering wing at zero angle of attack. The simulation extends beyond the time when the trailing edge of the wing exits the gust to ensure that the lift force returns to its steady-state value by the end of the simulation. As shown in Fig. 1, the wing experiences a lift overshoot after the leading edge enters the gust, and it lasts even after the trailing edge of the wing exits the gust. The lift coefficient then gradually returns to zero. Prior to one convective time, the lift values predicted by the LDVM (blue dashed line) show good agreement with experimental measurements (black line) taken in [40]. The experiments occurred with a NACA0012 wing of chord $c = 0.102$m and an effective aspect ratio of 5. The towing speed was 0.115m/s, and the Reynolds number was Re$= Uc/\nu = 12{,}000$. The LDVM over-predicts the peak value, but the remainder of the curve is generally close to the experimental data. For this paper, the LDVM serves as the test model in place of higher-fidelity simulations or experiments. Numerical simulations using the LDVM for maneuver optimization appear in Sect. 5.

## 3 Iterative maneuver optimization

The Iterative Maneuver Optimization (IMO) developed in [40] addresses the issue that optimal control profiles derived using a surrogate model of a wing–gust encounter fail to achieve their expected performance in experiments or higher-fidelity simulations due to the presence of unmodeled effects. The IMO method uses deviations of experimental measurements from the predicted aerodynamic forces to update the control signal. Through iterated application of this process, the control performance improves. This section briefly reviews the IMO method.

Let $u(t)$ with $t \in [t_0, t_f]$ be a scalar control signal between start time $t_0$ and end time $t_f$ that actuates the wing, and let $y_{\text{model}}$ represent a scalar force component of interest, such as lift. This paper investigates pitch and plunge accelerations individually as control inputs in Sect. 5. The IMO method requires a model for the dynamics of the system's state vector $\boldsymbol{x}$ in the form,

$$\dot{\boldsymbol{x}} = \boldsymbol{f}\left(\boldsymbol{x}, u, t; \boldsymbol{\mu}\right) \tag{1a}$$

$$y_{\text{model}} = h\left(\boldsymbol{x}, u, t; \boldsymbol{\mu}\right), \tag{1b}$$

where $\boldsymbol{f}$ and $h$ may be nonlinear functions, and $\boldsymbol{\mu}$ is a vector containing any empirical terms needed by the model. Equation (1) represents a surrogate model of the true dynamics of the fluid-wing interaction. The functions $\boldsymbol{f}$ and $h$ are assumed to be differentiable with respect to $\boldsymbol{x}$ and $u$ for optimal control calculations that are part of the IMO method. In prior work [40], an mGK model served as the surrogate model, and it contained numerous empirical terms that needed to be fit to the wing prior to use.

The IMO method performs an optimal control calculation to find a control signal $u$ that minimizes the performance index

$$J(u) = \frac{1}{2}\int_{t_0}^{t_f} \left(y_{\text{model}}^{(i)}\left(\boldsymbol{x}, u, t\right) - y_{\text{ref}}^{(i)}\right)^2 \mathrm{d}t, \tag{2}$$

subject to the dynamics of the surrogate model (1). The superscript $^{(i)}$ denotes that a signal comes from the $i$th iteration of the IMO method. On the first step of IMO, minimizing (2) regulates the model output $y^{(1)}_{\text{model}}$ to the constant value $y^{(1)}_{\text{ref}}$. On subsequent iterations, $y^{(i)}_{\text{ref}}$ becomes a non-constant signal that surrogate system should track. A candidate optimal control can be obtained by solving the first-order optimality conditions [49]

$$\dot{\boldsymbol{x}} = \left(\frac{\partial H}{\partial \boldsymbol{\lambda}}\right) \qquad \text{with} \quad \boldsymbol{x}\,(t_0) = \boldsymbol{x}_0 \tag{3a}$$

$$\dot{\boldsymbol{\lambda}} = -\left(\frac{\partial H}{\partial \boldsymbol{x}}\right)^T \quad \text{with} \quad \boldsymbol{\lambda}\left(t_f\right) = \mathbf{0} \tag{3b}$$

$$0 = \frac{\partial H}{\partial u}. \tag{3c}$$

Standard algorithms from optimal control theory (e.g., see [51]) can be used to solve the first-order optimality conditions (3). The authors' prior work [49] modifies these conditions to include terminal state constraints, which are useful if the wing is required to be in a particular configuration (i.e., position and orientation) at the end of the maneuver.

A control $u$ obtained by optimizing (2) over the surrogate model is tested in an experiment or high-fidelity simulation to produce the output signal $y^{(i)}_{\text{test}}(t)$ with $t \in [t_0, t_f]$. Although the model output $y^{(i)}_{\text{model}}$ is close to the reference value $y^{(i)}_{\text{ref}}$ as a result of the optimal control calculation, the output $y^{(i)}_{\text{test}}$ deviates from $y^{(i)}_{\text{ref}}$ due to unmodeled effects. The difference between the test (i.e., measured) output and the model output in the $i$th iteration is

$$\Delta y^{(i)} = y^{(i)}_{\text{test}} - y^{(i)}_{\text{model}}. \tag{4}$$

After completion of both surrogate optimization and testing of the control signal, if the absolute difference between the test signal and the reference $y^{(1)}_{\text{ref}}$ integrated over the time period is less a desired tolerance, then acceptable regulation has been achieved. Otherwise, the iteration counter is incremented such that $i = i + 1$ and the IMO process can continue.

The output error (4) can be used to find a new control signal in the next iteration by updating the reference signal for the optimal-control calculation to be

$$y^{(i)}_{\text{ref}} = y^{(1)}_{\text{ref}} - \Delta y^{(i-1)}. \tag{5}$$

IMO minimizes performance index (2) to track the new reference signal (5). Then, the updated optimal control profile can again be tested in experiment or high-fidelity simulation. To examine Eqs. (4) and (5) further, consider a force measurement $y^{(i)}_{\text{test}}$ at a given time that is less than the value predicted by the model $y^{(i)}_{\text{model}}$ due to unmodeled effects. Equations (4) and (5) would increase $y_{\text{ref}}$ for the next iteration, and the subsequent optimal-control calculation would seek a control that produces a larger model output $y_{\text{model}}$ at that time. If the surrogate model generally agrees with the true fluid dynamics, the subsequent test value $y_{\text{test}}$ should increase as well under the same control input, thereby bringing it closer to the initial reference value $y^{(1)}_{\text{ref}}$. This process repeats until the measured output signal $y_{\text{test}}$ approaches the constant, initial reference value $y^{(1)}_{\text{ref}}$. Figure 2 illustrates the IMO procedure.

The inputs to the algorithm are a time-averaged profile of the transverse gust, a surrogate model of the wing–gust interaction, and the reference output value for force regulation. The output of the algorithm is the optimal control input signal that achieves lift regulation. In prior work [40], the authors created a surrogate model by modifying a Goman–Khrabrov model to include effective angle of attack. Effective angle of attack allows for incorporation of a prescribed velocity field representing the gust. The output of the mGK model is the lift coefficient $C_L$, and the control input is pitch acceleration $\ddot{\theta}$. Using a DVM, the authors showed in simulation that the IMO method converges to produce an optimal, lift-regulating maneuver. The authors also experimentally tested the result in a water towing tank with a gust generator and showed that the IMO method approximately regulates lift in only a few iterations, similar to the numerical simulations. However, the final experimental iterations contained deviations from the reference lift that oscillated for further iterations. The authors showed that the same effect could be replicated in DVM by lowering the critical value of the leading edge suction parameter (i.e., the threshold for shedding at the leading edge) to make the leading edge more sensitive to shedding. Despite these small oscillations, experiments validated that the IMO method produces a lift-regulating pitch maneuver.

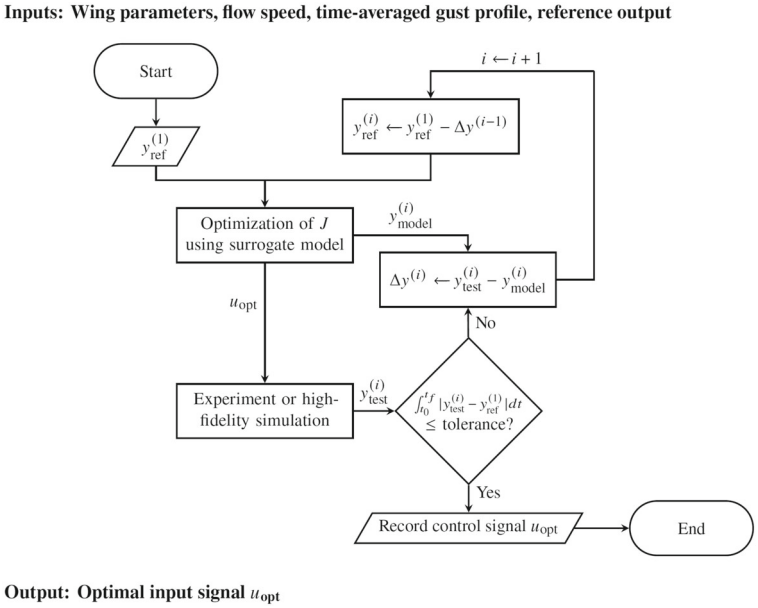


**Fig. 2** Iterative maneuver optimization (IMO) (Adapted from [40])

## 4 Simplified iterative maneuver optimization

This section introduces the Simplified Iterative Maneuver Optimization (SIMO) method. SIMO uses Theodorsen's lift model to eliminate the empirical terms in the mGK surrogate model and remove the requirement for a time-average profile of the gust. This change greatly reduces the experimental effort necessary before implementing the method. SIMO also replaces the costly optimization step in IMO with a more efficient simulation based on closed-loop tracking control of Theodorsen's lift model.

In [40], the IMO method uses a nonlinear mGK model that compares well to experimental lift measurements in the amplitude and duration of the lift overshoot for a non-maneuvering wing. However, the authors note that the mGK model also has a noticeable delay in the lift response when compared to experimental data. Despite this delay, IMO method is able to achieve accurate lift regulation. This observation suggests that the surrogate model does not need to be highly accurate, but simply adequate at capturing general trends of the system's response. A linear dynamic model may be sufficient when applied within the IMO framework.

One such linear dynamic model of lift is Theodorsen's unsteady lift model. Theodorsen's model predicts the lift coefficient of a wing undergoing pitching and plunging maneuvers based on expressions for added-mass and circulatory effects derived using potential-flow theory. Theodorsen's lift model is [52]

$$C_L = \pi b \left( \frac{\dot{\alpha}}{U} + \frac{\ddot{h}}{U^2} - \frac{ba\ddot{\alpha}}{U^2} \right) + 2\pi C(s) \left[ \frac{\dot{h}}{U} + \alpha + b\left(\frac{1}{2} - a\right) \frac{\dot{\alpha}}{U} \right], \tag{6}$$

where $b$ is the half-chord length, $U$ is the steady, free-stream velocity, $\alpha$ is the geometric angle of attack, $\dot{h}$ is the plunge rate, and $a$ is the location of the pitch axis in semi-chords (e.g., $a = -1$ indicates pitching about the leading edge and $a = 1$ is pitching about the trailing edge). $C(s)$ is a generalized version of *Theodorsen's function*, which is a complex-valued function that determines the effect of the trailing-edge wake on the circulatory contribution to the unsteady airloads [52]. This version of Theodorsen's function is generalized because it allows for arbitrary airfoil motions in addition to the sinusoidal motions originally considered by Theodorsen. There are several approximations to $C(s)$, and this paper uses R.T. Jones's approximation [17,41,53]

$$C(s) = \frac{0.5s^2 + 0.2808s + 0.01365}{s^2 + 0.3455s + 0.01365}, \tag{7}$$

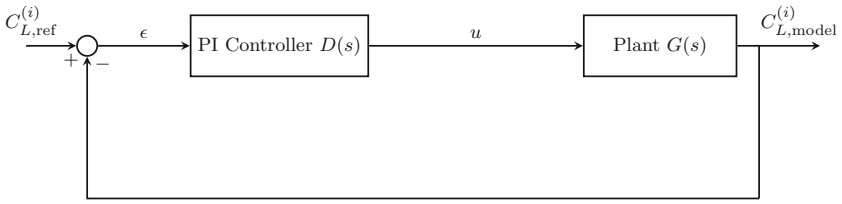


**Fig. 3** Closed-loop block diagram of the surrogate model

where $s$ is the Laplace variable. Using Theodorsen's model, Brunton and Rowley [41] calculate transfer functions from the pitch and plunge inputs to the lift coefficient output. Taking the Laplace transform $\mathscr{L}\{\cdot\}$ of Eq. (6), with zero initial conditions, and separating the pitch and plunge acceleration inputs yields

$$\begin{aligned}\mathscr{L}\{C_L\} = &\underbrace{\left(\frac{\pi b}{U}\left(\frac{1}{s} - ba\right) + 2\pi C(s)\left[\frac{1}{s^2} + \frac{b}{Us}\left(\frac{1}{2} - a\right)\right]\right)}_{G_\alpha(s)}\mathscr{L}\{\ddot{\alpha}\} \\ &+ \underbrace{\left(\frac{\pi b}{U^2} + C(s)\frac{2\pi}{Us}\right)}_{G_h(s)}\mathscr{L}\{\ddot{h}\},\end{aligned} \tag{8}$$

where the transfer function $G_\alpha(s)$ predicts the lift coefficient due to the pitch input, and $G_h(s)$ predicts the lift coefficient due to the plunge input. These transfer functions can serve as surrogate models for the wing.

The IMO method uses the surrogate model to generate an optimal input profile. For a constant reference input, the optimal control problem is a regulation problem. In subsequent iterations of IMO, the optimal control problem becomes a tracking problem because the surrogate model is required to track a reference lift signal that changes in time since it has been altered by the previous IMO iteration. The optimal control formalism and a gradient solution algorithm are necessary in IMO because the regulation and tracking problems use an mGK model, which is a nonlinear surrogate model. Since the optimization calculations are time-consuming, in the previous work [40], the authors noted that high-gain proportional feedback was capable of producing the optimal solution with less computation time. This observation suggests that a feedback control strategy may be able to provide the necessary tracking of the reference lift signal without the need for optimization. Instead, a controller that can adequately track the reference lift coefficient signal is all that is needed.

There are many approaches to design a tracking controller that can minimize deviations between $C_{L,\text{model}}$ and $C_{L,\text{ref}}$. One of the most common approaches is to use Proportional-Integral-Derivative (PID) control to compensate for the errors between the model output and the reference output. The control law can be expressed as

$$u(t) = K_p\epsilon(t) + K_i\int_0^t \epsilon(\tau)d\tau + K_d\frac{\mathrm{d}\epsilon(t)}{\mathrm{d}t}, \tag{9}$$

where $K_p$, $K_i$, $K_d$ are non-negative, constant gains corresponding to the proportional, integral, and derivative terms, respectively, and $\epsilon = C_{L,\text{ref}}^{(i)} - C_{L,\text{model}}^{(i)}$ is the tracking error. The control gains can be tuned in the closed-loop plant to make the model output closely match the reference signal. Note that it is not necessary to have all three terms in the PID controller. Only the proportional and integral terms are needed for good tracking of the Theodorsen lift model.

Figure 3 shows the block diagram for closed-loop tracking control of Theodorsen's model with unity feedback. The plant $G(s)$ represents Theodorsen's lift model, and the controller is a Proportional-Integral (PI) controller shown as $D(s)$, which is the Laplace transform of Eq. (9) with $K_d = 0$. Since this paper considers pitch and plunge acceleration inputs individually, the plant $G(s)$ represents either the $G_\alpha(s)$ or $G_h(s)$ transfer function, depending on the chosen input.

The transfer function from the reference $C_{L,\text{ref}}$ to the optimal maneuver $u$ can be computed based on the closed-loop system in Fig. 3 to be

$$P(s) = \frac{\mathscr{L}\{u(t)\}}{\mathscr{L}\{C_{L,\text{ref}}(t)\}} = \frac{D(s)}{1 + G(s)D(s)}. \tag{10}$$

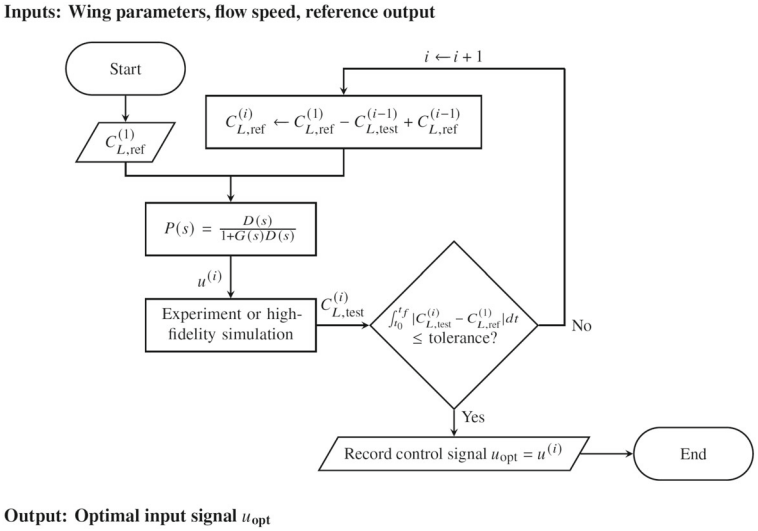


**Fig. 4** Simplified iterative maneuver optimization

Transfer function (10) can be used to find a control input $u(t)$ that causes the Theodorsen model to track the reference signal $C_{L,\mathrm{ref}}(t)$. Note that using transfer function (10) to generate a new input signal is equivalent to a closed-loop simulation of the PI controller acting on Theodorsen's lift model to make the wing closely track a reference lift signal. In this way, the closed-loop simulation (i.e., use of Eq. (10)) takes the place of the surrogate-model optimization that was previously performed in the IMO framework. The MATLAB command `lsim` readily implements this calculation to find $u(t)$, given $C_{L,\mathrm{ref}}(t)$.

The controller $D(s)$ should be tuned such that the closed-loop system $P(s)$ provides adequate tracking. If the output of the surrogate model $C_{L,\mathrm{model}}^{(i)}(t)$ identically tracks $C_{L,\mathrm{ref}}^{(i)}(t)$ (which is an acceptable assumption for a properly tuned controller), then an additional simplification to the IMO method is possible. Substituting Eq. (4) into Eq. (5) and replacing $C_{L,\mathrm{model}}^{(i-1)}$ with $C_{L,\mathrm{ref}}^{(i-1)}$ yields the reference signal update

$$C_{L,\mathrm{ref}}^{(i)} = C_{L,\mathrm{ref}}^{(1)} - C_{L,\mathrm{test}}^{(i-1)} + C_{L,\mathrm{ref}}^{(i-1)}. \tag{11}$$

Combining these simplifications results in the Simplified IMO (SIMO) algorithm, which appears in Fig. 4.

The surrogate model in SIMO is the Theodorsen's unsteady lift model with a PI controller that tracks the reference lift signal $C_{L,\mathrm{ref}}^{(i)}$. Although versions of Theodorsen's model with empirical factors exist (e.g., see [41]), the original model is derived from potential flow theory and does not contain empirical factors. Since the iterative process of updating the reference signal can compensate for some model inaccuracies, this paper uses the original form of Theodorsen's lift model to avoid empirical terms in the surrogate model. Treatment of the gust as a disturbance further reduces empirical fitting, because it eliminates the need for prior knowledge of the gust profile in the surrogate model.

In the SIMO method, the wing discovers the gust on the first iteration during collection of $C_{L,\mathrm{test}}^{(1)}$. Unlike the IMO method, for which the initial maneuver is based on optimal regulation of the surrogate mGK model, SIMO does not maneuver the wing on the first iteration. This paper assumes that the wing operates at the reference lift value $C_{L,\mathrm{ref}}^{(1)}$ prior to the gust encounter. Since the surrogate model does not contain gust effects, the PI controller continues to hold the wing's initial configuration for the duration of iteration 1. The gust acts as an additive output disturbance that occurs in the experiment or high-fidelity simulation and causes the lift to differ from the expected response. After the reference lift signal is disturbed by the first test run, the PI controller acts to track an updated reference lift signal that encodes disturbance information on the next iteration. The SIMO method proceeds with additional iterations until $C_{L,\mathrm{test}}^{(i)}$ matches $C_{L,\mathrm{ref}}^{(1)}$ within an acceptable tolerance. For the numerical simulations in this work, the tolerance was set to $5 \times 10^{-4}$ for both pitching and plunging motions. The value of the error $\int |C_{L,\mathrm{test}}^{(i)} - C_{L,\mathrm{ref}}^{(1)}| \mathrm{d}t$ in Fig. 4 should also be monitored to identify occurrences of oscillations that prevent further decrease in the error.

This paper applies the SIMO method to the problem of a wing encountering a transverse gust. However, SIMO may also be applicable to other problems in fluid dynamics that focus on lift regulation via wing maneuvering, provided that the external flow field can be reliably replicated in each iteration of the experiments.

## 5 Numerical simulations

This section numerically implements the SIMO method from Sect. 4 in LDVM simulations of transverse gust encounters to produce optimized maneuvers for pitch or plunge acceleration inputs.

### 5.1 Pitch maneuver optimization

In the authors' prior work on the IMO method [40], the wing generally performed a pitch-down and then, pitch-up maneuver to mitigate the lift overshoot during a transverse gust encounter. The authors found that for an LESPc value of 0.18, the IMO method converges in simulation to nearly perfect regulation of $C_L$ to zero within seven iterations. For an LESPc value of 0.12, the authors found oscillations in the maneuver updates, preventing further convergence of the solution after several iterations. Therefore, the present paper focuses on the more challenging case of LESPc$=0.12$ for investigation of the SIMO method and comparison with the IMO method.

To numerically implement SIMO for a pitch acceleration input, the simulation parameters are set to match experimental values in the previous work [40]. The freestream flow speed, which is based on the towing speed of the wing, is 0.115m/s, and the gust ratio is approximately GR$=0.7$. The chord length of the wing is $c = 0.102$m. The pitch axis location is on the chord line at $a = -0.17$. The control input is pitch acceleration $\ddot{\theta}$, and the output is lift coefficient $C_L$. To generate control signals based on tracking control of the surrogate model, the proportional and integral control gains in (9) were selected to be $K_p = 1.4$ and $K_i = 435.24$, respectively, for all iterations. These values were selected using the `pidtune` command in MATLAB with a 0dB open-loop crossover frequency of 50Hz. The crossover frequency was selected to be at a sufficiently larger value than the greatest anticipated frequency of aerodynamic effects and actuation signals. Note that plotting of the reference signal $C_{L,\text{ref}}$ and the output signal $C_{L,\text{model}}$ after a tracking simulation can verify good tracking performance for the selected gains or aid in gain tuning.

Figure 5 presents pitch maneuver optimization using the SIMO method. The non-dimensional pitch rate and pitch acceleration are $\dot{\theta}_g^* = \dot{\theta}_g c/U$ and $\ddot{\theta}_g^* = \ddot{\theta}_g c^2/U^2$, respectively. No maneuvering occurred on the first iteration, producing a lift-overshoot profile as shown in Fig. 5a. The second iteration applied a pitch-down maneuver to counteract the lift overshoot. However, this maneuver was too strong and produced a lift undershoot instead. In iteration 3, the wing reduced the maneuvering amplitude, eliminating the lift undershoot and producing less lift overshoot than the non-maneuvering case. Iterations 4 through 8 continued to reduce deviations from the desired value of $C_L = 0$. However, small oscillations in the solution at $t^* = 1.8$ were noticed and the simulation was terminated due to a lack of improvement beyond iteration 8. Iteration 8 was selected as an optimal result. The largest absolute deviation in lift coefficient for iteration 10 was 0.08, which represents a 97% reduction in maximum lift deviation compared to iteration 1.

Figure 5b shows the angle of attack maneuver for each iteration, as well as the pitch acceleration input that generates the maneuver. The optimized maneuver on iteration 8 is a pitch-down, then pitch-up maneuver as shown in Fig. 5b. Figure 6 compares the optimized lift responses of the IMO method (blue line) and the SIMO method (red line). These lines are taken from optimal iteration for each method, and it is clear that SIMO method performed better than the IMO method at generating a lift-regulating maneuver. The simpler Theodorsen model may be better suited than the mGK model to serve as a surrogate in iterative maneuver optimization.

These simulation results show that the SIMO method is capable of optimizing the maneuver of a pitching wing in a transverse gust for lift regulation. Similar to IMO, SIMO also exhibits oscillation in the optimized maneuver after several iterations. Oscillation of the maneuver is the subject of ongoing work for improvement of the method. Nevertheless, the SIMO method rapidly generates an optimized maneuver in only a few iterations of maneuvering in the LDVM simulation. Further, SIMO outperforms the IMO method for this simulation and does so without prior knowledge of the gust profile.

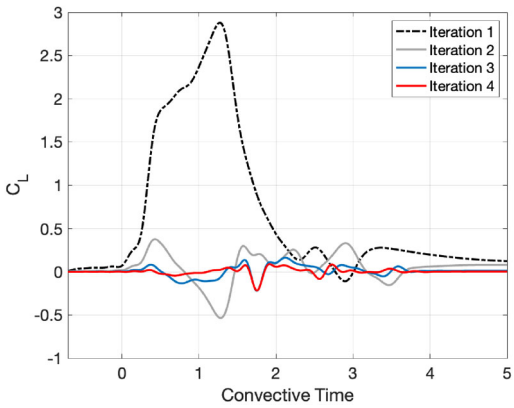


**a** Iterations 1 to 4

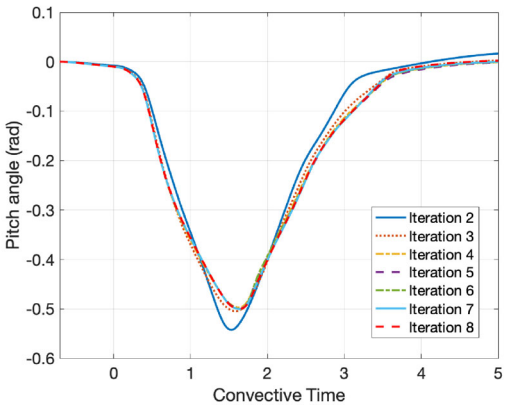


**b** Pitch angles

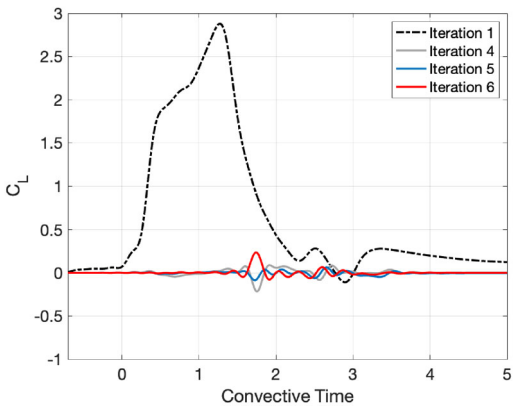


**c** Iterations 4 to 6

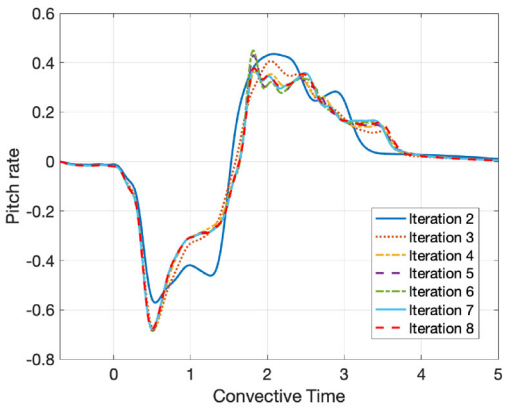


**d** Pitch rates

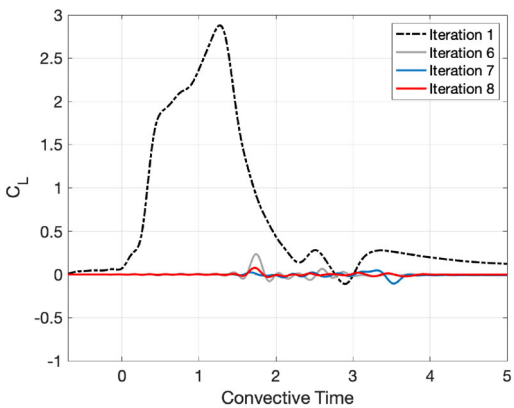


**e** Iterations 6 to 8

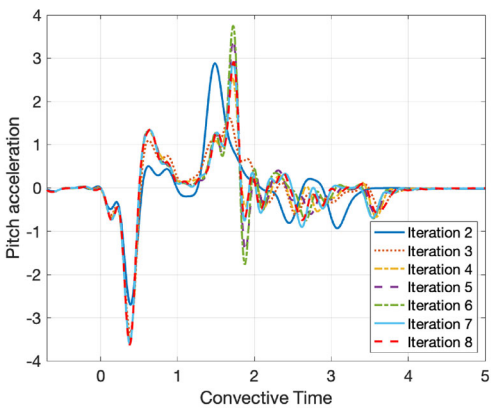


**f** Pitch accelerations

**Fig. 5** LDVM simulation results of the SIMO method for a pitch acceleration input

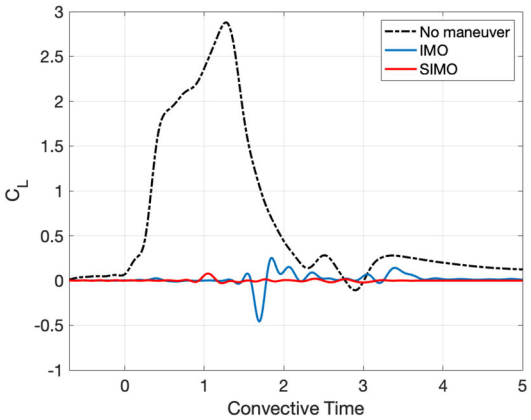


**Fig. 6** Comparison of lift regulation for maneuvers generated using the IMO and SIMO methods

## 5.2 Plunge maneuver optimization

This numerical simulation investigates lift regulation using a plunge acceleration input to derive a plunge maneuver. Theodorsen's lift model decomposes into the transfer functions from pitch and plunge inputs to the lift output in Eq. (8). To examine plunge individually, the pitch input was set to zero. The simulation parameters for wing geometry and flow conditions, including the LESPc value, matched those from the numerical simulation in Sect. 5.1 for pitch maneuvering. The PI controller in the surrogate tracking model was tuned to control gains of $K_p = 0$ and $K_i = 4.13$ for all iterations, which shows that only integral control was active.

Figure 7 presents the lift response results for plunge maneuver optimization using the SIMO method. The non-dimensional plunge amplitude, plunge rate, and plunge acceleration are $h^* = h/c$, $\dot{h}^* = \dot{h}/U$, and $\ddot{h}^* = \ddot{h}c/U^2$, respectively. For iteration 1 in Fig. 7a, the wing did not maneuver, which provided the same open-loop gust response seen in the previous numerical simulation. For iteration 2, the plunge motion derived by SIMO significantly reduced the largest absolute deviation in lift coefficient to 0.4, which is an 86% reduction from the non-maneuvering wing's lift overshoot. Notably, the plunge maneuver from iteration 2 mitigated the disturbance similar to the pitching maneuver from iteration 2 in Fig. 5a. The remaining iterations in Fig. 7c, e continued to refine the performance of the plunge maneuver in small increments. By iteration 8, the largest absolute deviation of the lift coefficient was 0.02, which is a reduction of 99% from the open-loop lift overshoot. Within an acceptable tolerance, iteration 8 optimally regulated the lift coefficient to zero during the gust encounter through the use of a plunge maneuver. Note that the plunge maneuver required fewer iterations than the pitch maneuver to optimize, and it did not experience significant oscillation of the lift signal with continued iteration.

Figure 7b, f record the plunge amplitudes and accelerations, respectively. The plots show rapid convergence of the plunge maneuver after iteration 2. The optimal plunge maneuver can generally be described as negatively plunging (i.e., ascending) to a higher altitude and holding the new position. The wing ascended to approximately $-0.1$m and held that amplitude after $t^* = 3$. The optimal plunge input in Fig. 7f is negative for downward acceleration during entry into the gust and positive after exiting the gust to bring the plunge rate back to zero. In contrast to the optimized pitch maneuver, which returned the wing to its original orientation after the gust encounter, the optimal plunge maneuver held an offset altitude after the encounter. Since the angle of attack is explicitly in Theodorsen's lift model in Eq. (6), the wing naturally returns to its initial orientation at the end of the pitch maneuver for lift regulation. That is, when all rate-of-change terms in Eq. (6) go to zero, the angle of attack must match the initial angle of attack for the lift value to be the same. Note that the plunge rate and plunge acceleration appear in Eq. (6), but the plunge amplitude does not. This observation reveals a benefit of the IMO framework over the SIMO method, because IMO incorporates terminal constraints on the final configuration of the wing in the optimization portion of the mGK surrogate model.

Figure 8 depicts the free vortices in the flow field for four time instants during the LDVM simulations in a reference frame that translates horizontally with the wing. Each row shows the plunge maneuver for an iteration of the SIMO method. Iteration 1 shows the non-maneuvering gust encounter. A large LEV rolls up during entry into the gust and sheds shortly after $t^* = 1.1$. The negative plunging or ascending motion in the

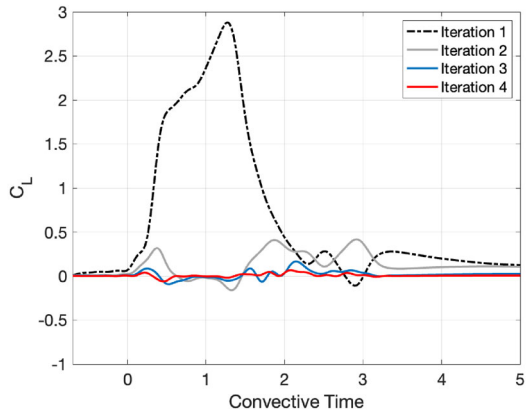


**a** Iterations 1 to 4

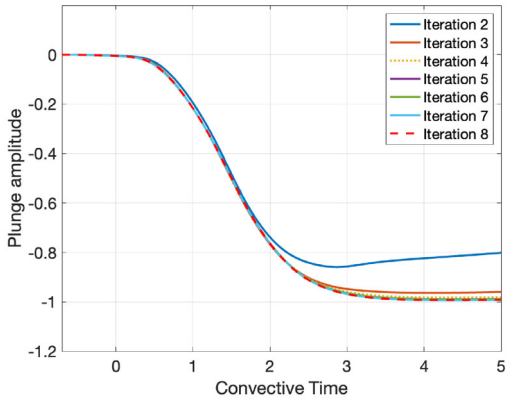


**b** Plunge amplitudes

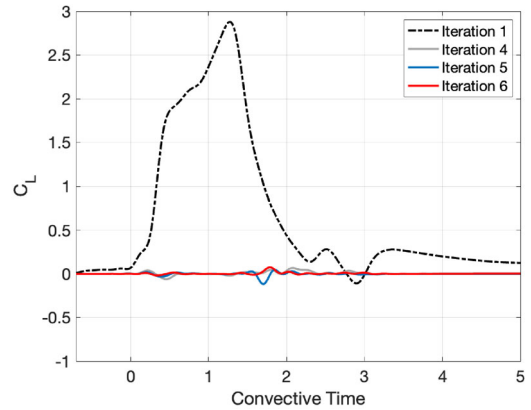


**c** Iterations 4 to 6

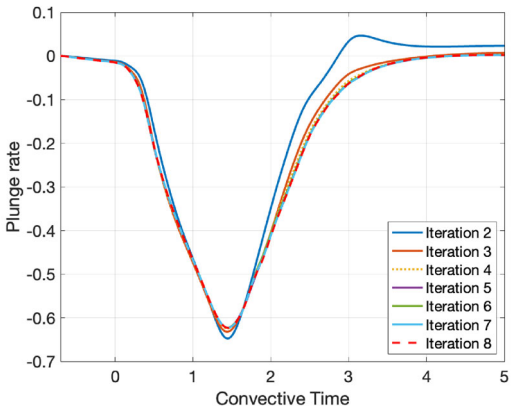


**d** Plunge rates

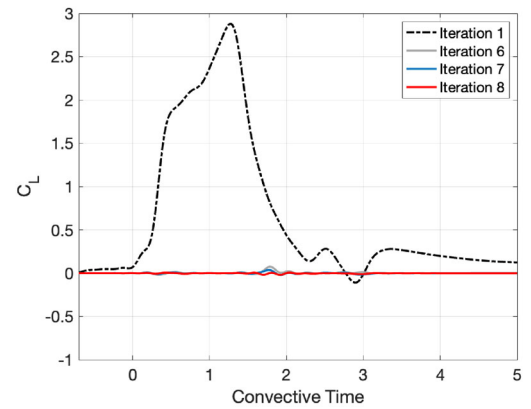


**e** Iterations 6 to 8

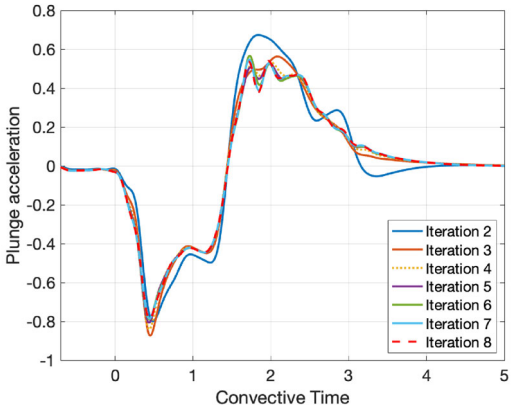


**f** Plunge accelerations

**Fig. 7** SIMO of a wing–gust encounter in LDVM simulation and the corresponding plunging maneuvers

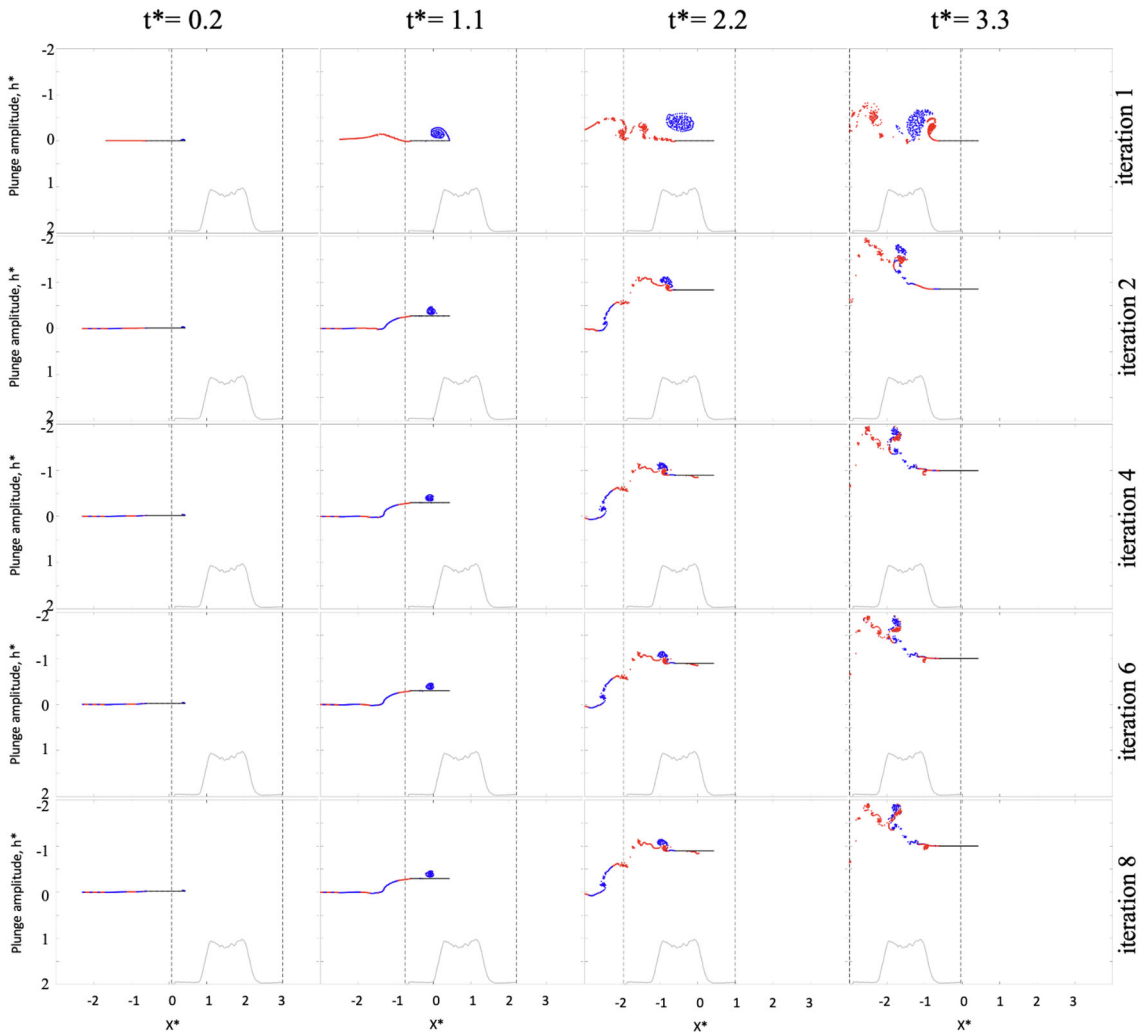


**Fig. 8** Free vortices in the flow field for SIMO iterations with a plunge acceleration input. The view is in the wing's body-frame, with the wing moving from left to right

SIMO iterations reduces the size of the LEV and causes shedding of the LEV before $t^* = 1.1$. Also, note that at time instant $t^* = 2.2$, the wake from vortex shedding at the trailing edge is reduced in iteration 8 as compared to iteration 1.

After iteration 2, a small LEV advects under the high-pressure side of the wing and can be seen at $t^* = 2.2$. The high-pressure side LEV is often present for pitch maneuvers. Figure 9 compares the optimized pitch and plunge maneuvers at $t^* = 2.2$, and it shows a smaller high-pressure-side LEV appears for the plunge maneuver than the pitch maneuver. The less prominent high-pressure-side LEV may account for the improved lift regulation of the plunge maneuver. Figure 9c, d shows the LESP profiles during the simulation for the plunging maneuver and the pitching maneuver, respectively. The LESP values of pitching and plunging both reached the negative critical value, which resulted in LEV shedding at the pressure side of the wing. However, the plunge maneuver had a shorter time period of LEV shedding in comparison with the pitch maneuver.

## 6 Experimental results

This section presents experimental validation of the SIMO method for both pitching and plunging maneuvers, by replacing the DVM simulations of the previous section with experimental force measurements in SIMO framework in Fig. 4. Experiments were carried out in a free-surface water towing tank at the University of Maryland (UMD) that is outfitted with a custom, transverse-gust generation system. The dimensions of the

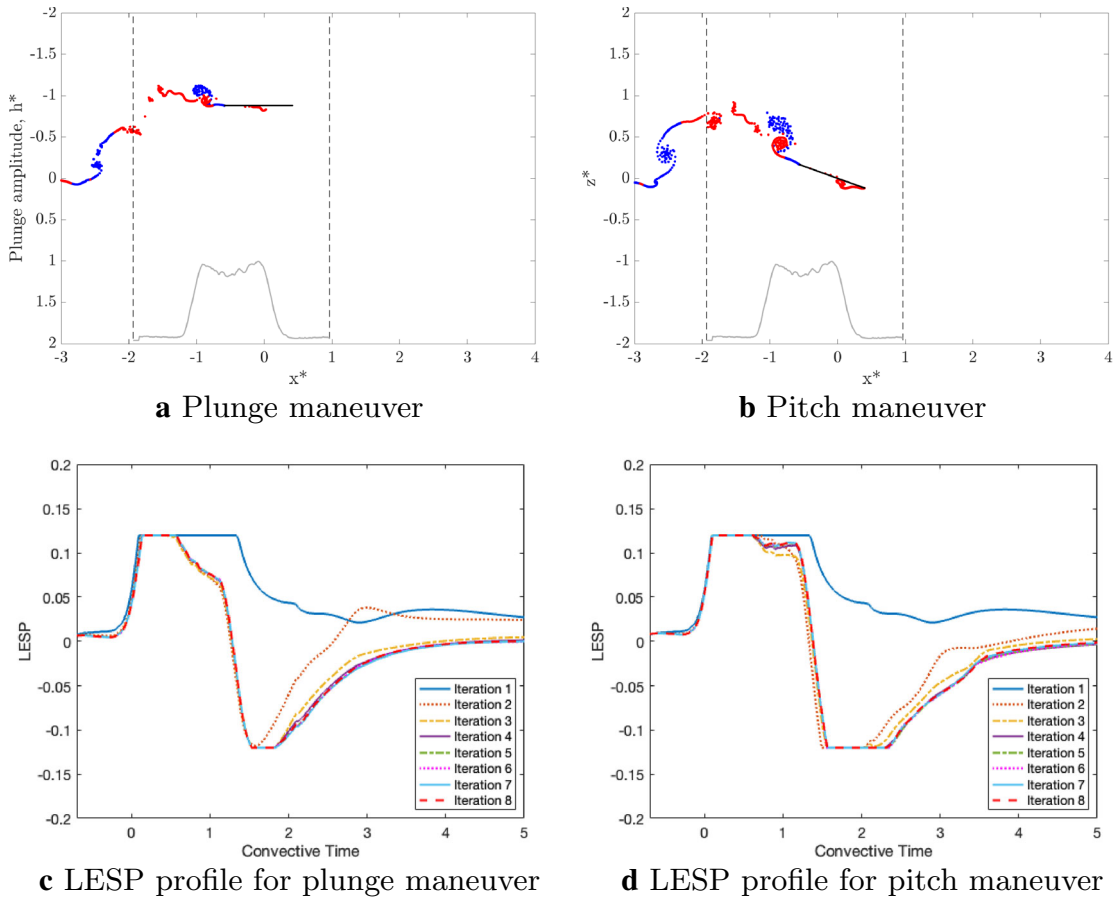


**a** Plunge maneuver **b** Pitch maneuver

**c** LESP profile for plunge maneuver **d** LESP profile for pitch maneuver

**Fig. 9** **a** and **b** Comparison of free vortices in the flow field of the LDVM simulation at $t^* = 2.2$. **c** and **d** LESP time history during LDVM simulations

tank are 7 m long, 1.5 m wide, and 1m deep. A NACA 0012 profile was used for the wing model with a chord of 0.102 m and a span of 0.254 m. Experiments were conducted at Reynolds number 12,000. Force measurements were filtered by a low-pass filter with a cutoff frequency of 5 Hz and were ensemble-averaged over five runs for each iteration in the SIMO method. Additional details of the experimental setup can be found in [40].

Figure 10 shows the experimental results of the SIMO method for a pitching wing. Figure 10a presents the coefficient of the measured lift force, and Fig. 10b–d shows the pitch kinematics for all iterations of the SIMO method. During the first iteration, the wing did not maneuver and a strong lift overshoot was recorded, similar to the numerical simulation in Fig. 1. On iteration 2, the wing performed a pitch-down and then, pitch-up maneuver, similar iteration 2 of the numerical simulation in Fig. 5. As a result, the wing significantly reduced the lift-overshoot during the gust encounter, although a small lift-undershoot was observed after $t^* = 1.5$ and a second lift overshoot occurred after $t^* = 2.5$. These two deviations were also observed in the LDVM simulations. Iterations 3 through 5 further improved lift regulation during the gust encounter and overcame the second lift-overshoot in iteration 2. After iteration 5, no further improvement of lift regulation was observed with additional iteration. Iteration-to-iteration oscillation of the lift signal occurred, similar to the finding reported in the IMO method of [40]. The experiment was terminated and the input signal from iteration 5 was taken as the optimized input signal since the maximum absolute lift coefficient had been mitigated to 0.13, representing a 96% reduction in the uncontrolled lift overshoot. Further convergence of the lift signal may not be possible due to motor vibration effects that are not modeled in the surrogate model for maneuver updating, as was previously noted by the authors in [40]. Figure 10b shows that the wing pitched down and then, pitched up to mitigate the lift overshoot. The SIMO method efficiently produced a near-optimal pitch profile after iteration 2. Variations in the pitch rate and pitch acceleration produced small adjustments to the overall pitch profile after iteration 2.

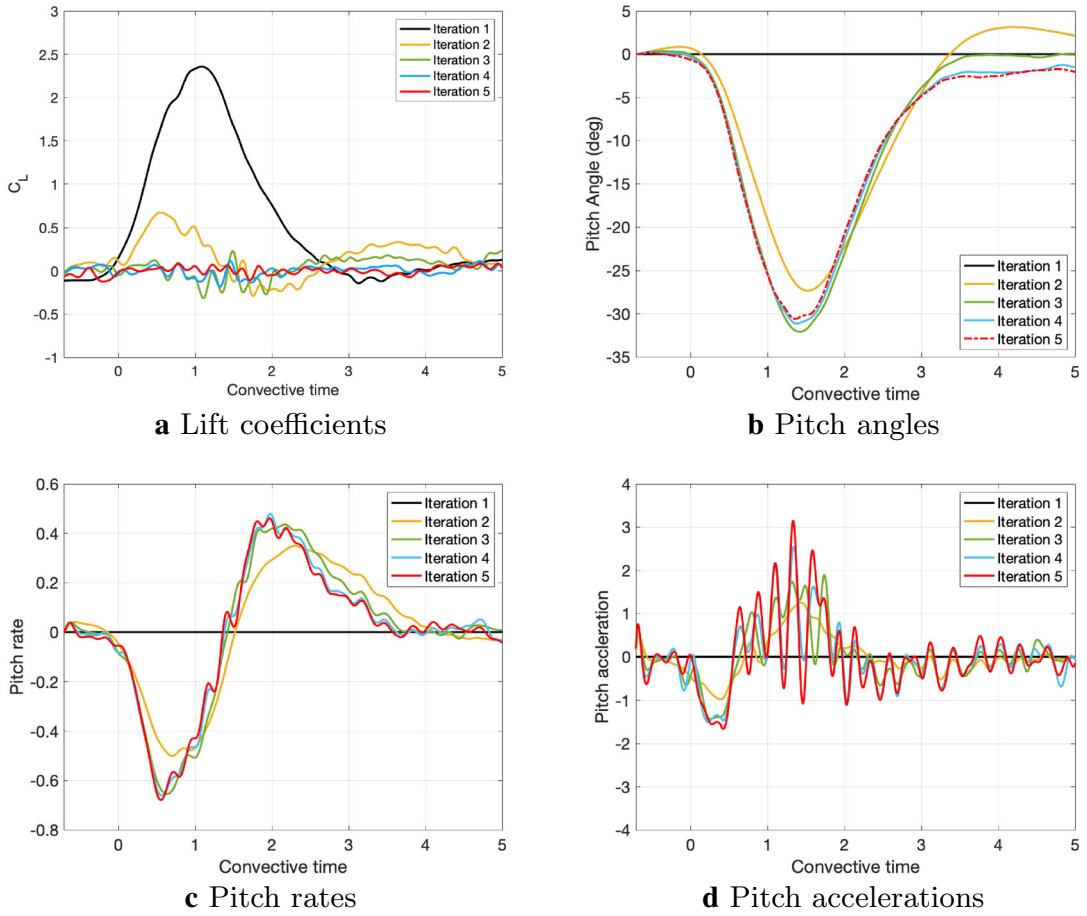


**a** Lift coefficients **b** Pitch angles

**c** Pitch rates **d** Pitch accelerations

**Fig. 10** Experimental results of the SIMO method for a pitch acceleration input

In addition to pitching, the experimental setup (see details in [40]) permits change in elevation of the wing through the actuation of the rods that hold the wing model in the tow tank setup. For the fixed pitch angle of zero degrees, plunge experiments were conducted to test the SIMO method for plunge acceleration inputs. Figure 11 presents the results of SIMO iterations in the gust encounter. By iteration 2, the maximum lift coefficient was reduced to 0.25 during the gust encounter, although a secondary lift overshoot with a peak value of 0.37 occurred at $t^* = 3$ after exiting the gust. Iterations 3 and 4 continued to decreased the absolute deviations in lift. However, for subsequent iterations, further convergence of the lift signal was not observed—iteration-to-iteration oscillation occurred. Comparison of the lift signal from iteration 4 to iteration 5 provides an example of the lift oscillation for continued iteration.

Overall, the wing applied a reverse plunge maneuver to increase its altitude, as shown in Fig. 11b. Note that the maximum value of the optimal plunge rate in Fig. 7d was very close to the peak value of the gust velocity, indicating that the optimal plunge maneuver may correspond to the vehicle ascending with the gust. Notably, the plunge amplitude showed good convergence in the iterations during the first half of the experiment for $t^* < 2$. However, after $t^* = 2$, the plunge amplitude signal in experiments did not converge as it did in the simulations of Fig. 7b. The continued movement of the plunge amplitude curve could be attributed to the presence of shed vorticity in the flow near the wing that has not yet been carried far from the wing. Previous research [54] has linked the secondary lift peak after exiting the gust with shed vorticity on the upper surface of the wing. Increasing the duration of the experiment for all iterations may be a possible solution to address this issue, by allowing more time for the shed vorticity to advect. Iteration 4 was selected as the optimized plunge profile since its lift deviations were small and the plunge amplitude leveled-off to constant amplitude with a near-zero plunge rate. Iteration 4 reduced the maximum absolute deviation in lift coefficient to 0.2, which represents a 92% reduction from the uncontrolled wing in iteration 1. Overall, the plunge experiments

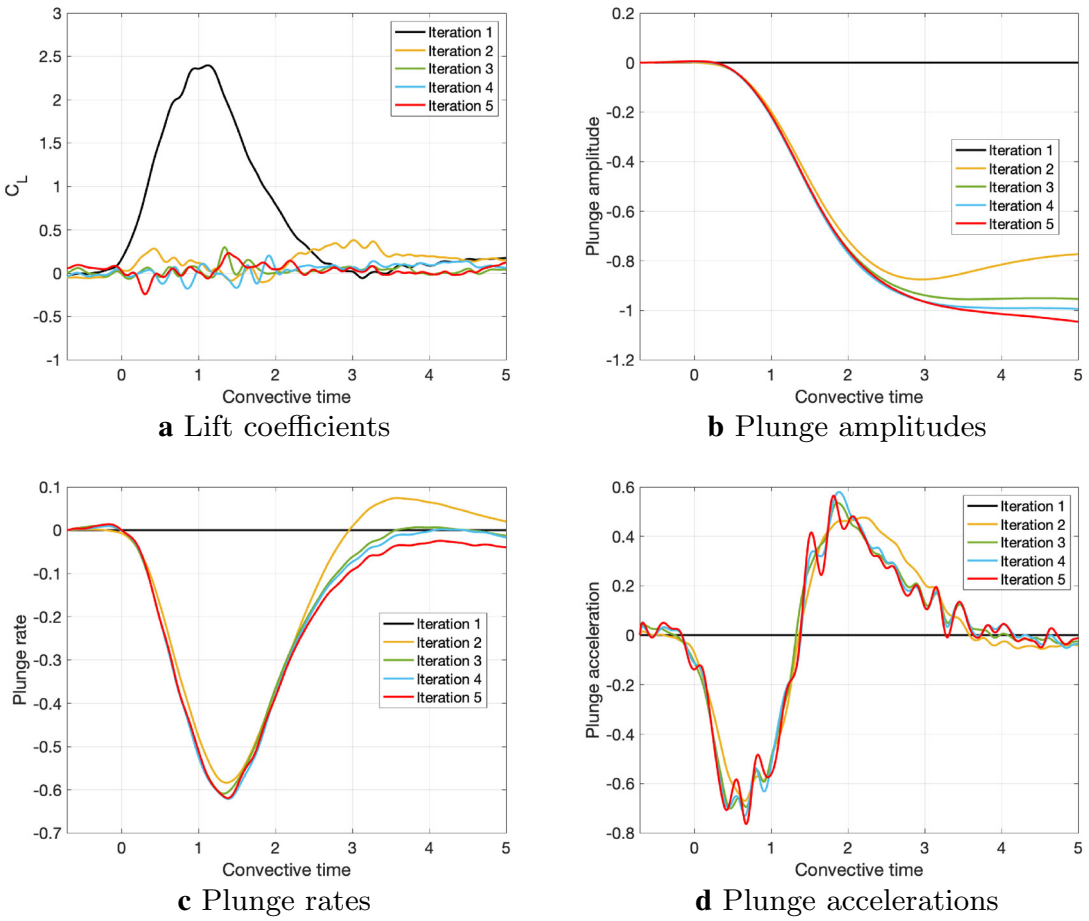


**a** Lift coefficients **b** Plunge amplitudes

**c** Plunge rates **d** Plunge accelerations

**Fig. 11** Experimental results of the SIMO method for a plunge acceleration input

demonstrated that the SIMO method can optimize a plunge maneuver in a transverse gust encounter. Another direction for future investigation is extension of the SIMO method to other types of disturbances.

## 7 Conclusion

This work revises and simplifies the Iterative Maneuvering Optimization (IMO) framework developed in the authors' previous work in [40]. IMO is a tool to create lift-regulating maneuvers by conducting several successive experiments or numerical simulations. A Simplified Iterative Maneuvering Optimization (SIMO) method is introduced and tested in this paper with numerical simulations using a discrete vortex model. The SIMO method replaces optimization over a surrogate model in the IMO method with Theodorsen's unsteady lift model combined with a PI controller to track a reference lift signal. Additionally, the new SIMO approach does not require any preliminary experimental effort to obtain empirical parameters for a surrogate model or the time-averaged profile of the external flow field, which is required by IMO. These changes significantly simplify the IMO framework.

The SIMO method can be used for pitching or plunging maneuvers, and both numerical simulations and experiments successfully generated the optimal inputs for lift regulation during a transverse gust encounter for a trapezoidal gust profile. The wing applies a pitch-down, then pitch-up maneuver for pitch actuation and a negative plunge (i.e., ascent) motion for plunge actuation. In the numerical simulations, the resulting pitch maneuver provides a 97% reduction in the maximum absolute lift response, and the plunge maneuver provides 99% reduction. Snapshots of the vorticity field of the plunge case indicate that the optimal maneuver reduces shedding of vorticity at the leading edge during the encounter. In the experiments, the optimal pitch maneuver

achieved a 96% reduction while the plunge maneuver achieved a 92% reduction in the maximum absolute lift response.

Future work will include a stability analysis of the SIMO method and PIV measurements of the flow fields of the pitch and plunge maneuvers during the SIMO process. Since the current implementation of SIMO only considers pitching from a zero initial pitch angle, investigating nonzero initial pitch angles and tracking of non-constant reference signals will be subjects for future work. Extension of SIMO to other forms of disturbances would also be interesting.

**Acknowledgements** This work was supported by the National Science Foundation under grant CBET-2003999, monitored by program officer R. Joslin. The authors gratefully acknowledge valuable discussions with Z. Chen, J. Graff, A. SureshBabu, A. Gopalarathnam, and J. Hrynuk.

**Author contribution** Xianzhang Xu created the theoretical optimization framework and wrote the manuscript. Antonios Gementzopoulos conducted the experimental validation and contributed to manuscript preparation. Girguis Sedky constructed the experimental setup and contributed to manuscript preparation. Anya R. Jones performed experimental design and contributed to manuscript preparation. Francis D. Lagor designed the numerical experiments, reviewed the research findings, and supervised preparation of the manuscript.

**Funding** This work was supported by the National Science Foundation under grants CBET-2003951 and CBET-2003999, monitored by program officer R. Joslin.

**Availability of data and materials** Not applicable.

**Declarations**

**Conflict of interest** Not applicable.

**Ethical approval** Not applicable.

## References

1. Zarovy, S., Costello, M., Mehta, A., Gremillion, G., Miller, D., Ranganathan, B., Humbert, J.S., Samuel, P.: Experimental study of gust effects on micro air vehicles. In: AIAA Atmospheric Flight Mechanics Conference, p. 7818 (2010)
2. Moulin, B., Karpel, M.: Gust loads alleviation using special control surfaces. J. Aircr. **44**(1), 17–25 (2007)
3. Moriche, M., Flores, O., Garciá-Villalba, M.: On the aerodynamic forces on heaving and pitching airfoils at low Reynolds number. J. Fluid Mech. **828**, 395–423 (2017). https://doi.org/10.1017/jfm.2017.508
4. Sedky, G., Gementzopoulos, A., Andreu-Angulo, I., Lagor, F.D., Jones, A.R.: Physics of gust response mitigation in open-loop pitching manoeuvres. J. Fluid Mech. **944**, 38 (2022). https://doi.org/10.1017/jfm.2022.509
5. Jones, A.R., Cetiner, O., Smith, M.J.: Physics and modeling of large flow disturbances: discrete gust encounters for modern air vehicles. Annu. Rev. Fluid Mech. **54**, 469–493 (2021). https://doi.org/10.1146/annurev-fluid-031621-085520
6. Bhatia, M., Patil, M., Woolsey, C., Stanford, B., Beran, P.: Stabilization of flapping-wing micro-air vehicles in gust environments. J. Guid. Control. Dyn. **37**(2), 592–607 (2014). https://doi.org/10.2514/1.59875
7. Cook, R.G., Palacios, R., Goulart, P.: Robust gust alleviation and stabilization of very flexible aircraft. AIAA J. **51**(2), 330–340 (2013)
8. Oduyela, A., Slegers, N.: Gust mitigation of micro air vehicles using passive articulated wings. Sci. World J. **2014** (2014)
9. Jones, A.R.: Gust encounters of rigid wings: Taming the parameter space. Phys. Rev. Fluids **5**(11), 110513 (2020)
10. Ellington, C.P., den Berg, C.V., Willmott, A.P.: Leading-edge vortices in insect flight. Nature **384**(December), 626–630 (1990)
11. Biler, H., Badrya, C., Jones, A.R.: Experimental and computational investigation of transverse gust encounters. AIAA J. **57**(11), 1–15 (2019). https://doi.org/10.2514/1.j057646
12. Grubb, A.L., Moushegian, A., Heathcote, D.J., Smith, M.J.: Physics and computational modeling of nonlinear transverse gust encounters. In: AIAA SciTech 2020 Forum (2020). https://doi.org/10.2514/6.2020-0080
13. Andreu-Angulo, I., Babinsky, H., Biler, H., Sedky, G., Jones, A.R.: Effect of transverse gust velocity profiles. AIAA J. **58**(12), 5123–5133 (2020)
14. Andreu-Angulo, I., Babinsky, H.: Mitigation of airfoil gust loads through pitch. AIAA J. **60**(9), 5273–5285 (2022)
15. Sedky, G., Jones, A.R., Lagor, F.D.: Lift regulation during transverse gust encounters using a modified Goman–Khrabrov model. AIAA J. **58**(9), 1–11 (2020). https://doi.org/10.2514/1.J059127
16. Xu, X., Lagor, F.D.: Optimal pitching in a transverse gust encounter using a modified goman-khrabrov model. In: AIAA AVIATION 2021 FORUM, p. 2937 (2021)
17. Sedky, G.: Mitigation of transverse gusts via open- and closed-loop pitching maneuvers. Ph.D. dissertation, University of Maryland (2022)
18. Theodorsen, T., Mutchler, W.: General theory of aerodynamic instability and the mechanism of flutter (1935)
19. Wagner, H.: Über die entstehung des dynamischen auftriebes von tragflügeln. ZAMM-J. Appl. Math. Mech./Zeitschrift für Angew. Math. und Mech. **5**(1), 17–35 (1925)

20. Küssner, H.G.: Zusammenfassender bericht über den instationären auftrieb von flügeln. Luftfahrtforschung **13**(12), 410–424 (1936)
21. von Kármán, T.: Airfoil theory for non-uniform motion. J Aeronaut. Sci. **5**(10), 379–390 (1938). https://doi.org/10.2514/8.674
22. Sedky, G., Gementzopoulos, A., Andreu-Angulo, I., Lagor, F.D., Jones, A.R.: Physics of gust response mitigation in open-loop pitching manoeuvres. J. Fluid Mech. **944**, 38 (2022)
23. Corkery, S.J., Babinsky, H.: An investigation into gust shear layer vorticity and the added mass force for a transverse wing-gust encounter. In: AIAA Scitech 2019 Forum, p. 1145 (2019)
24. Katz, J., Plotkin, A.: Low-Speed Aerodynamics, vol. 13, 2nd edn. Cambridge University Press, Cambridge (2001)
25. Ramesh, K., Gopalarathnam, A., Granlund, K., Ol, M.V., Edwards, J.R.: Discrete-vortex method with novel shedding criterion for unsteady aerofoil flows with intermittent leading-edge vortex shedding. J. Fluid Mech. **751**, 500–538 (2014). https://doi.org/10.1017/jfm.2014.297
26. Andreu Angulo, I., Babinsky, H.: Negating gust effects by actively pitching a wing. In: AIAA Scitech 2020 Forum, p. 1057 (2020)
27. Sedky, G., Lagor, F.D., Jones, A.: Unsteady aerodynamics of lift regulation during a transverse gust encounter. Phys. Rev. Fluids **5**, 074701 (2020). https://doi.org/10.1103/PhysRevFluids.5.074701
28. Goman, M., Khrabrov, A.: State-space representation of aerodynamic characteristics of an aircraft at high angles of attack. J. Aircr. **31**(5), 1109–1115 (1994). https://doi.org/10.2514/3.46618
29. Milano, M., Gharib, M.: Uncovering the physics of flapping flat plates with artificial evolution. J. Fluid Mech. **534**, 403–409 (2005)
30. Peng, D., Milano, M.: Lift generation with optimal elastic pitching for a flapping plate. J. Fluid Mech. **717** (2013)
31. Quinn, D.B., Lauder, G.V., Smits, A.J.: Maximizing the efficiency of a flexible propulsor using experimental optimization. J. Fluid Mech. **767**, 430–448 (2015)
32. Berkooz, G., Holmes, P., Lumley, J.L.: The proper orthogonal decomposition in the analysis of turbulent flows. Annu. Rev. Fluid Mech. **25**(1), 539–575 (1993)
33. Schmid, P.J.: Dynamic mode decomposition of numerical and experimental data. J. Fluid Mech. **656**, 5–28 (2010)
34. Rowley, C.W., Dawson, S.T.: Model reduction for flow analysis and control. Annu. Rev. Fluid Mech. **49**(1), 387–417 (2017)
35. Williams, M.O., Kevrekidis, I.G., Rowley, C.W.: A data-driven approximation of the Koopman operator: extending dynamic mode decomposition. J. Nonlinear Sci **25**(6), 1307–1346 (2015). https://doi.org/10.1007/s00332-015-9258-5
36. Proctor, J.L., Brunton, S.L., Kutz, J.N.: Dynamic mode decomposition with control. SIAM J. Appl. Dyn. Syst. **15**(1), 142–161 (2016)
37. Deem, E.A., Cattafesta, L.N., Hemati, M.S., Zhang, H., Rowley, C., Mittal, R.: Adaptive separation control of a laminar boundary layer using online dynamic mode decomposition. J. Fluid Mech. **903** (2020)
38. Hjalmarsson, H., Gevers, M., Gunnarsson, S., Lequin, O.: Iterative feedback tuning: theory and applications. IEEE Control Syst. Mag. **18**(4), 26–41 (1998)
39. Uchiyama, M., Mihara, M.: Determination of malonaldehyde precursor in tissues by thiobarbituric acid test. Anal. Biochem. **86**(1), 271–278 (1978)
40. Xu, X., Gementzopoulos, A., Sedky, G., Jones, A.R., Lagor, F.D.: Iterative maneuver optimization in a transverse gust encounter. AIAA J., pp. 1–17 (2023)
41. Brunton, S.L., Rowley, C.W.: Empirical state-space representations for Theodorsen's lift model. J. Fluids Struct. **38**, 174–186 (2013)
42. Xia, X., Mohseni, K.: Unsteady aerodynamics and vortex-sheet formation of a two-dimensional airfoil. J. Fluid Mech. **830**, 439–478 (2017)
43. Narsipur, S., Gopalarathnam, A., Edwards, J.R.: Low-order model for prediction of trailing-edge separation in unsteady flow. AIAA J. **57**(1), 191–207 (2019). https://doi.org/10.2514/1.J057132
44. Xia, X., Mohseni, K.: Lift evaluation of a two-dimensional pitching flat plate. Phys. Fluids **25**(9), 091901 (2013)
45. SureshBabu, A.V., Medina, A., Rockwood, M., Bryant, M., Gopalarathnam, A.: Theoretical and experimental investigation of an unsteady airfoil in the presence of external flow disturbances. J. Fluid Mech. **921** (2021). https://doi.org/10.1017/jfm.2021.484
46. SureshBabu, A.V., Ramesh, K., Gopalarathnam, A.: Model reduction in discrete-vortex methods for unsteady airfoil flows. AIAA J. **57**, 1409–1422 (2019). https://doi.org/10.2514/1.J057458
47. Xu, X., Lagor, F.D.: Simplified iterative maneuver optimization in a transverse gust encounter. In: AIAA SCITECH 2023 Forum, p. 2478 (2023)
48. Narsipur, S., Hosangadi, P., Gopalarathnam, A., Edwards, J.R.: Variation of leading-edge suction during stall for unsteady aerofoil motions. J. Fluid Mech. **900**, 25 (2020). https://doi.org/10.1017/jfm.2020.467
49. Xu, X., Lagor, F.D.: Quasi-steady effective angle of attack and its use in lift-equivalent motion design. AIAA J. **59**(7), 1–14 (2021). https://doi.org/10.2514/1.J059663
50. Hemati, M.S., Eldredge, J.D., Speyer, J.L.: Improving vortex models via optimal control theory. J. Fluids Struct. **49**, 91–111 (2014)
51. Bryson, A.E., Ho, Y.-C.: Applied Optimal Control: Optimization, Estimation, and Control, 1st edn. Routledge, London (1975)
52. Leishman, G.J.: Principles of Helicopter Aerodynamics, 2nd edn. Cambridge University, Cambridge (2006)
53. Jones, R.T.: Operational treatment of the nonuniform-lift theory in airplane dynamics. Technical report (1938)
54. Perrotta, G., Jones, A.R.: Unsteady forcing on a flat-plate wing in large transverse gusts. Exp. Fluids **58**, 1–11 (2017)